Journal of Materials Chemistry C

ROYAL SOCIETY OF CHEMISTRY

PAPER

View Article Online
View Journal | View Issue

Cite this: J. Mater. Chem. C, 2021, 9, 5198

Anthracene-based bipolar deep-blue emitters for efficient white OLEDs with ultra-high stabilities of emission color and efficiency†

Xiangyu Zhu,[a] Yinghao Li,[a] Zilong Wu,[a] Chengwei Lin,[a] Dongge Ma,[a] Zujin Zhao *[a] and Ben Zhong Tang[abc]

Received 29th January 2021,
Accepted 18th March 2021

DOI: 10.1039/d1tc00432h

rsc.li/materials-c

Blue organic luminescent materials are important because of their applications in illumination and full-color displays, but those with high efficiency and stable emission are insufficient. Herein, two new luminescent compounds, 10-(4-(10-(4-(carbazol-9-yl)phenyl)-2,6-di-*tert*-butylanthracen-9-yl)phenyl)-9,9-dimethyl-9,10-dihydroacridine (**Cz-TAn-DMAC**) and 4-(2,6-di-*tert*-butyl-10-(4-(9,9-dimethylacridin-10-yl)phenyl)anthracen-9-yl)-*N*,*N*-diphenylaniline (**TPA-TAn-DMAC**), comprising *tert*-butyl-modified anthracene, dimethyl acridine and carbazole or triphenylamine groups are successfully synthesized, and their thermal stability, optical property, electronic structure, and electrochemical behavior are measured and analyzed. They exhibit efficient deep-blue emissions in neat films and bipolar carrier transport ability. The non-doped OLED based on **TPA-TAn-DMAC** provides bright deep-blue light ($CIE_{x,y}$ = 0.14, 0.18) with a high external quantum efficiency (η_{ext}) of 4.9%, and the doped OLED of **Cz-TAn-DMAC** radiates blue light ($CIE_{x,y}$ = 0.15, 0.08) with a η_{ext} of 4.8%. In addition, two-color hybrid warm white OLEDs with high-performance are fabricated by using **TPA-TAn-DMAC** as the blue emission layer, thus achieving ultra-high stability, efficiency and color at high luminance over 10 000 cd m^{-2}, indicative of a very promising OLED application prospect.

Introduction

Currently, more and more displays and smart phones have shifted from liquid crystal display panels to organic light-emitting diodes (OLEDs) panels due to various advantages of OLEDs such as wide color gamut, self-luminescence, thinness, and flexibility. In addition to display, white OLEDs (WOLEDs) have the virtues of surface emission, low blue, soft light, sun-like light, and no dazzle, which make them promising candidates as next-generation lighting sources.[1–9] However, the lighting products based on WOLEDs have not been adopted on a wide scale because of the exorbitant price and inferior brightness and stability. The explorations on robust luminescent materials, optimum device configurations and advanced fabrication techniques are of vital importance.[10–12]

So far, among many device configurations for WOLEDs, hybrid WOLEDs using a blue fluorophore and red, green, or orange phosphors have been extensively studied because of the efficient utilization of excitons for radiative decay and spectra-stable emission. Because phosphorescent OLEDs can theoretically achieve 100% internal quantum efficiency, the performances of hybrid WOLEDs are often determined by blue fluorescent components.[13–17] In 2014, Zheng *et al.*, fabricated fluorescence-phosphorescence hybrid WOLEDs with a total external quantum efficiency (η_{ext}) of 21%.[18] In 2018, Ma *et al.* used a deep-blue molecule with aggregation-induced emission (AIE) as the blue emitter and a phosphor host to fabricate WOLEDs, thus achieving a η_{ext} of 19.6% at 1000 cd m^{-2}.[2] In the same year, Lee *et al.* reported hybrid WOLEDs created by doping a yellow phosphor into blue fluorescent material and a maximum η_{ext} of 27.5% was realized.[19] However, the decreased efficiency at high luminance remains in most cases. In fact, although a few blue fluorescent emitters have obtained the maximum η_{ext} values reaching 10.7%,[20] a majority of the blue fluorescent emitters are still not satisfactory in terms of low electroluminescence (EL) efficiency, poor color purity, and weak stability, which undermine the performance of WOLEDs to a large degree. Hence, the development of blue emitters with high efficiency and high stability has always been attractive but challenging.[21–24]

[a] State Key Laboratory of Luminescent Materials and Devices, Guangdong Provincial Key Laboratory of Luminescence from Molecular Aggregates, SCUT-HKUST Joint Research Institute, South China University of Technology, Guangzhou, 510640, China. E-mail: mszjzhao@scut.edu.cn
[b] Department of Chemistry, The Hong Kong University of Science and Technology Clear Water Bay, Kowloon, Hong Kong, China
[c] AIE Institute, Guangzhou Development District, Huangpu, Guangzhou 510530, China

† Electronic supplementary information (ESI) available: General information, synthesis and characterization of target compounds, devices fabrication and measurement, TGA curves, PL spectra in different solvents, PL and EL decay curves, CV curves, and MEL response curves. See DOI: 10.1039/d1tc00432h

To achieve deep-blue light and high EL efficiency, anthracene derivatives are often used as building blocks owing to the easy chemical modification and excellent photoluminescence (PL) property.[25–29] However, because of the rigid and planar structure, the anthracene group tends to form a close π–π stacking, which will lead to PL quenching in the aggregated state, and thus weaken the EL efficiency. To avoid such a situation, the chemical introduction of twisted or branched groups onto the molecules is often adopted to inhibit the close packing of molecules.[30–35] Hence, to achieve deep-blue emission and high PL efficiency, the 9,10-positions of the anthracene is substituted with relatively weak donor/acceptor with twisted structures.[36–43] In this work, two custom-tailored anthracene derivatives (**TPA-TAn-DMAC** and **Cz-TAn-DMAC**) are designed and prepared. These compounds are equipped with the branched *tert*-butyl and the nonplanar 9,9-dimethyl-9,10-dihydroacridine (DMAC) groups to get out of the state of close molecular packing in the aggregated state. Moreover, to enhance the carrier transport ability, carbazole (Cz) and triphenylamine (TPA) groups are introduced. Consequently, **Cz-TAn-DMAC** and **TPA-TAn-DMAC** exhibit efficient deep-blue emissions in the solid-state. Notably, they can not only function efficiently in non-doped and doped deep-blue OLEDs but also serve as blue component to create high-performance two-color hybrid WOLEDs with superb spectral stability and extremely low efficiency roll-off.

Results and discussion

Synthesis and characterization

Scheme 1 shows the synthetic routes towards these new blue compounds, **Cz-TAn-DMAC** and **TPA-TAn-DMAC**. Compounds **1**–**5** were prepared by the reported methods.[25,29,44] **Cz-TAn-DMAC** and **TPA-TAn-DMAC** were synthesized using Suzuki couplings of **3** with **4** and **5**, respectively, in good yields. All final products were completely characterized by NMR and high-resolution mass spectroscopy, which are described in the ESI.† Both **Cz-TAn-DMAC** and **TPA-TAn-DMAC** have good solubility in dichloromethane, chloroform, tetrahydrofuran (THF) and toluene, but poor solubility in water. **Cz-TAn-DMAC** and **TPA-TAn-DMAC** have high decomposition temperatures (T_ds) of 467 and 446 °C, respectively, at 5% loss of initial weight (Fig. S1, ESI†). Such a good thermal stability is favoured to fabricate high-performance OLEDs using the vacuum-deposition technique.

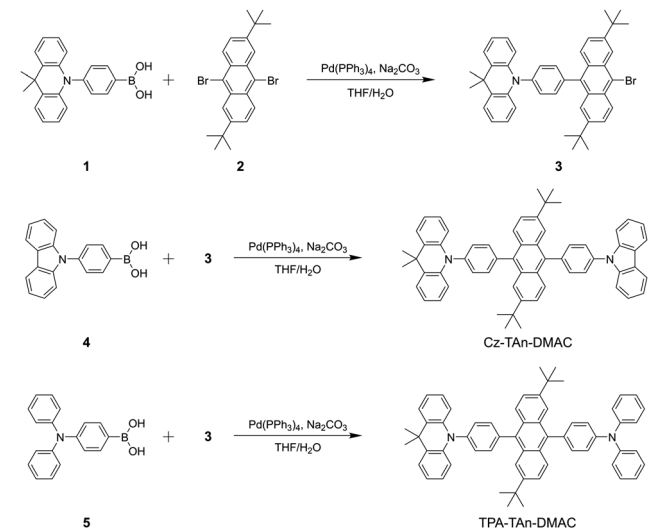

Scheme 1 Molecular structures and synthetic routes of **Cz-TAn-DMAC** and **TPA-TAn-DMAC**.

Photophysical properties

Cz-TAn-DMAC and **TPA-TAn-DMAC** show similar absorption maxima at ~393 nm (Fig. 1A) in dilute THF solution (10 μM), because of the π–π* transition of the planar anthracene core. From the absorption onsets, the optical bandgaps (E_gs) are deduced to be 2.90 and 2.86 eV for **Cz-TAn-DMAC** and **TPA-TAn-DMAC**, respectively. The PL spectra of **Cz-TAn-DMAC** and **TPA-TAn-DMAC** in the dilute THF solution (10 μM) and their evaporated films are shown in Fig. 1B. In THF solutions, **Cz-TAn-DMAC** and **TPA-TAn-DMAC** have deep blue PL emissions with peaks at 436 and 464 nm and fluorescence quantum yields (Φ_Fs) of 60.2% and 50.7%, respectively. The redder PL emission and lower Φ_F of **TPA-TAn-DMAC** than **Cz-TAn-DMAC** can be ascribed to its stronger intramolecular charge transfer (ICT)[45] in the polar THF solution because of the stronger electron-donating ability of TPA than Cz, which is evidenced by the solvatochromism experiment (Fig. S2, ESI†). In vacuum-deposited neat films, the PL peak of **Cz-TAn-DMAC** is located at 449 nm, which is red-shifted by 13 nm than that in the THF solution, and the Φ_F is decreased to 41.7%. This should be caused by close packing among the planar carbazole groups and thus enhanced intermolecular interaction in the neat film. By doping **Cz-TAn-DMAC** in CBP (4,4′-bis(carbazol-9-yl)biphenyl) host at a concentration of 10 wt%, the PL peak is blue-shifted to 440 nm and the Φ_F is increased to 74.5%, owing to the reduced intermolecular interaction as well as rigidified molecular structure by spatial constraint.[46] Compared with THF solution, neat and doped films of **TPA-TAn-DMAC** show bluer PL peaks at 459 and 457 nm and higher Φ_F values of 53.7% and 71.5%, respectively, because of the structure rigidification in the film state and the branched TPA group that can better suppress close packing. PL

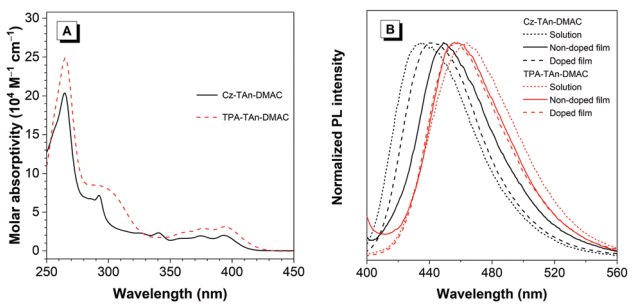

Fig. 1 (A) Absorption spectra of **Cz-TAn-DMAC** and **TPA-TAn-DMAC** in THF solutions (1×10^{-5} M). (B) Photoluminescence (PL) spectra of **Cz-TAn-DMAC** and **TPA-TAn-DMAC** in THF solutions, neat films and doped films (in CBP host at 10 wt% concentration).

Table 1 Photophysical properties, thermal stabilities, and energy levels of the new compounds

Compound	λ_{abs} (nm)	λ_{em} (nm)		Φ_F[b] (%)		HOMO/LUMO[c] (eV)	E_g[d] (eV)	T[e] (ns)		T_d (°C)
		THF	Neat/doped film[a]	THF	Neat/doped film[a]			THF	Neat film	
Cz-TAn-DMAC	393	436	449/440	67.2	41.7/74.5	−5.18/−2.28	2.90	5.49	3.67	467
TPA-TAn-DMAC	394	464	459/457	50.7	53.7/71.5	−5.16/−2.30	2.86	2.63	2.52	446

[a] Evaporated solid neat film and doped film in CBP host at a concentration of 10 wt%. [b] Absolute fluorescence quantum yield determined by a calibrated integrating sphere. [c] Determined by cyclic voltammetry. [d] Optical bandgap calculated from the onset of absorption spectrum. [e] Fluorescence lifetime, measured at room temperature in air.

decay curves of both the compounds are measured in THF solutions and neat films under ambient conditions (Fig. S3, ESI†). The PL lifetimes of **Cz-TAn-DMAC** and **TPA-TAn-DMAC** in THF solutions are 5.49 and 2.63 ns, respectively, which are very close to those in the neat films (3.67 and 2.52 ns) (Table 1), indicative of their fluorescent nature and the absence of dimer-like state, which will result in a longer PL lifetime.

Theoretical calculation

To demonstrate the electronic structures, the optimized structure for the lowest singlet (S_1) states of **Cz-TAn-DMAC** and **TPA-TAn-DMAC** are calculated by the M06-2X/6-31G* basis set. As shown in Fig. 2, they have relatively twisted conformations, and the dihedral angles of anthracene plane and DMAC are relatively large (54.41° for **Cz-TAn-DMAC**, and 55.67° for **TPA-TAn-DMAC**). The twisted conformation and the presence of *tert*-butyl groups can avert close molecular stacking, which inhibits strong molecular interactions and ensures efficient emission in the aggregated states. To identify their transition characteristic, the natural transition orbital (NTO) analysis for the optimized S_1 states is calculated by M06-2X/6-311G*. The holes and particles of the two compounds are primarily localized on anthracene, indicative of the great contribution of anthracene to luminescence. The intramolecular charge transfer effect should be weak in both these compounds, which is conducive to obtaining deep-blue emissions.

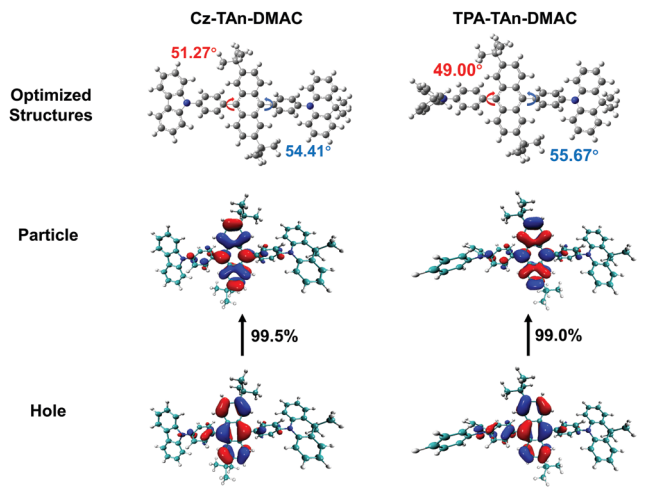

Fig. 2 Natural transition orbital analysis for the S_1 states based on ground state optimized structures of **Cz-TAn-DMAC** and **TPA-TAn-DMAC**, calculated by M06-2X/6-31G* and M06-2X/6-311G* basis set. The predominant wave functions of hole and particle with the largest weight are illustrated.

Electrochemical behaviours

To investigate the electrochemical property, cyclic voltammetric (CV) measurement was conducted on **Cz-TAn-DMAC** and **TPA-TAn-DMAC** (Fig. S4, ESI†). Both the compounds show reversible oxidation processes, with onset oxidation potentials (E_{ox}) of 0.64 and 0.62 V for **Cz-TAn-DMAC** and **TPA-TAn-DMAC**, respectively. Thus, the highest occupied molecular orbital (HOMO) energy levels of **Cz-TAn-DMAC** and **TPA-TAn-DMAC** are calculated to be −5.18 and −5.16 eV by the equation of HOMO = (E_{ox} + 4.8 − $E_{ox,fc}$) (eV), in which the E_{ox} value of F_c/F_c^+ ($E_{ox,fc}$) is 0.26 V. The HOMO energy levels of **Cz-TAn-DMAC** and **TPA-TAn-DMAC** are close to those of the commonly used hole-transporting materials, such as 4,4′-bis(1-naphthylphenylamino)biphenyl (NPB, −5.2 eV),[47] which benefits the hole injection and transport. While the energy levels of the lowest unoccupied molecular orbital (LUMO) are −2.28 and −2.30 eV, for **Cz-TAn-DMAC** and **TPA-TAn-DMAC**, respectively, determined by the equation of LUMO = HOMO + E_g, where E_g is the optical bandgap obtained from the onset of the UV absorption spectrum.

Electroluminescence

Because of the good PL efficiencies in neat films and high thermal stability of both the compounds, non-doped OLEDs with a simple configuration of ITO/NPB (40 nm)/emitter (20 nm)/2,2′,2″-(1,3,5-benzinetriyl)tris(1-phenylbenzimidazole) (TPBI) (40 nm)/LiF (1 nm)/Al (120 nm) are fabricated, where the emitter is **Cz-TAn-DMAC** (device B1) or **TPA-TAn-DMAC** (device B2), and NPB and TPBI are employed as the hole-transporting and electron-transporting layers, respectively (Fig. 3A). The devices B1 and B2 radiate blue EL emissions peaking at 442 nm ($CIE_{x,y}$ = 0.17, 0.15) and 462 nm ($CIE_{x,y}$ = 0.14, 0.18), respectively, which are close to their PL emissions in solid films, thus confirming that the exciton recombination occurs in the emitting layer and the EL emissions result from radiative decay of the singlet excitons. Device B1 shows good EL performance with maximum luminance (L_{max}) of 5026 cd m^{-2}, maximum current efficiency ($\eta_{C,max}$) of 3.8 cd A^{-1}, maximum power efficiency ($\eta_{p,max}$) of 2.9 lm W^{-1}, and maximum external quantum efficiency ($\eta_{ext,max}$) of 3.5%. Moreover, because of the higher solid-state Φ_F of **TPA-TAn-DMAC**, device B2 displays better EL performance with L_{max} of 9070 cd m^{-2}, $\eta_{C,max}$ of 6.2 cd A^{-1}, $\eta_{P,max}$ of 5.7 lm W^{-1}, and $\eta_{ext,max}$ of 4.9%. These good EL performances are comparable to those of the efficient deep-blue fluorescent OLEDs

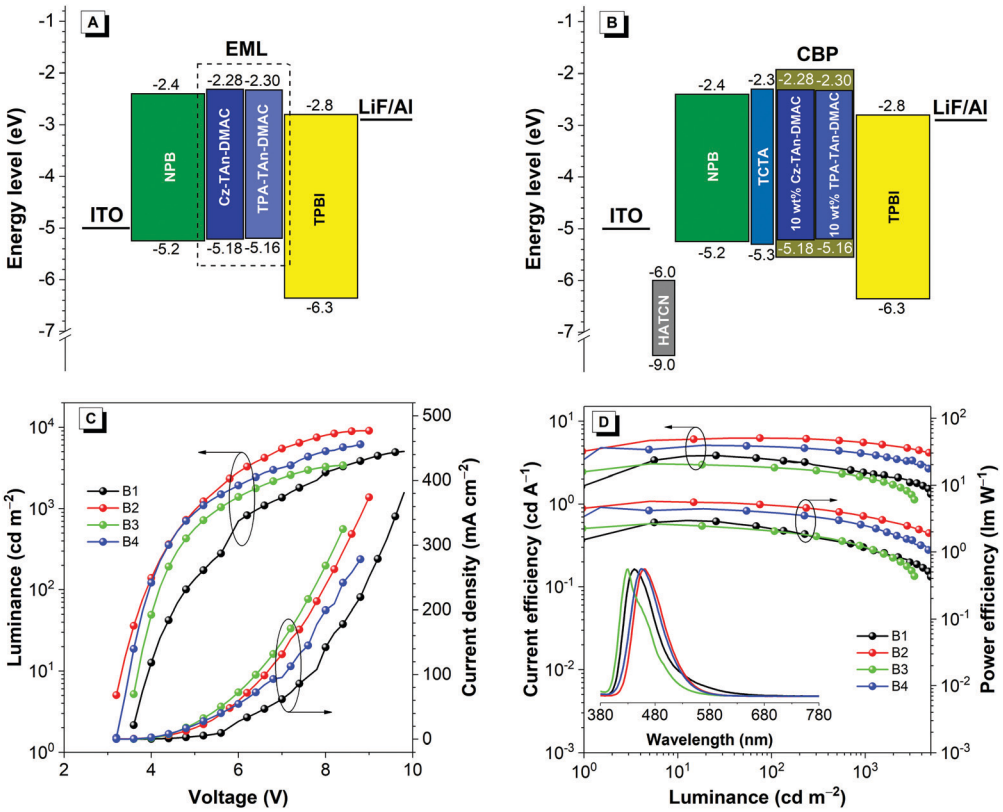

Fig. 3 Device structures and energy diagrams of (A) non-doped devices B1 and B2 and (B) doped devices B3 and B4 using **Cz-TAn-DMAC** and **TPA-TAn-DMAC** as emitters, respectively. (C) Curves of luminance–voltage–current density of devices B1–B4. (D) Plots of current efficiency and power efficiency–luminance of devices B1–B4. Inset: EL spectra of devices B1–B4 at 10 mA cm^{-2}.

in the literature (Table S1, ESI†), and are highly indicative of the great potential of both compounds as emitters for non-doped blue OLEDs.

The theoretical value of the radioactive exciton ratio can be calculated using the equation $\eta_{ext} = \Phi_F \cdot \eta_{exciton} \cdot \eta_{eh} \cdot \eta_{out}$, where η_{ext} is the external quantum efficiency, $\eta_{exciton}$ is the exciton utilization efficiency, η_{out} is the light out-coupling efficiency (*ca.* 20–30%), and η_{eh} is the recombination efficiency of the holes and electrons, which is ideally assumed as 100%. According to the equation, the $\eta_{exciton}$ values of non-doped devices based on **Cz-TAn-DMAC** and **TPA-TAn-DMAC** are in the ranges of 28–42% and 30–46%, respectively. These $\eta_{exciton}$ values are higher than the theoretical limit of 25%, which is probably due to the triplet–triplet fusion (TTF).[18] To confirm the TTF mechanism, the transient EL spectra of the non-doped devices are measured (Fig. S5, ESI†), in which the delayed EL components can be obviously observed. To distinguish that the delayed EL originated from the TTF process rather than the recombination of trapped charges,[48,49] the magneto-electroluminescence (MEL) effect is studied. The MEL responses of two non-doped devices at multiple voltages are shown in Fig. S6 (ESI†). With increase in voltage, the line shapes of MEL change obviously, with an increase at low voltages and then a decrease at high voltages, indicating the existence of TTF process in the EL process,[50–53] which accounts for the higher $\eta_{exciton}$ values than the theoretical limit.

To further investigate the EL performances of both the compounds, the doping technique is used, and doped OLEDs with a configuration of ITO/1,4,5,8,9,11-hexaazatriphenylenehexacarbonitrile (HATCN) (5 nm)/NPB (40 nm)/tris(4-carbazoyl-9-ylphenyl) amine (TCTA) (5 nm)/emitters (20 nm)/TPBI (40 nm)/LiF (1 nm)/Al (120 nm) are fabricated, in which HATCN and TCTA work as the hole injection and exciton-blocking layers, respectively, and the emitter comprised the doped film of **Cz-TAn-DMAC** (device B3) or **TPA-TAn-DMAC** (device B4) in CBP host at a concentration of 10 wt% (Fig. 3B). The doped device B3 of **Cz-TAn-DMAC** radiates stable deep-blue EL emission with a peak at 434 nm ($CIE_{x,y}$ = 0.15, 0.08) at 1000 cd m^{-2}, which is very close to the blue standard of the National Television Standards Committee (NTSC),[54,55] and shows high L_{max}, $\eta_{C,max}$, $\eta_{P,max}$, $\eta_{ext,max}$ of 4324 cd m^{-2}, 3.1 cd A^{-1}, 2.8 lm W^{-1}, and 4.8%, respectively. $\eta_{ext,max}$ is obviously improved compared with that of the non-doped device, revealing that **Cz-TAn-DMAC** is more suitable for doped devices because of the higher Φ_F in the doped film than in the neat film. The L_{max}, $\eta_{C,max}$, $\eta_{P,max}$, and $\eta_{ext,max}$ of doped device B4 of **TPA-TAn-DMAC** are 6152 cd m^{-2}, 5.1 cd A^{-1}, 4.4 lm W^{-1}, and 4.7%, which are close to those of the non-doped device, demonstrating that **TPA-TAn-DMAC** can efficiently function in both the doped and non-doped OLEDs (Table 2).

Carrier transport

Concerning the excellent EL performance of the two compounds, its carrier transport ability is investigated by the

Table 2 EL performance of **Cz-TAn-DMAC** and **TPA-TAn-DMAC** based deep-blue OLEDs

Device	V_{on}[a] (V)	η_C[b] (cd A^{-1})	η_P[b] (lm W^{-1})	η_{ext}[b] (%)	L[c] (cd m^{-2})	CIE[d] (x, y)	λ_{EL}[d] (nm)
B1	3.6	3.8/2.4	2.9/1.2	3.5/2.2	5026	(0.17, 0.15)	442
B2	3.2	6.2/5.5	5.7/3.4	4.9/4.3	9070	(0.14, 0.18)	462
B3	3.4	3.1/2.5	2.8/1.3	4.8/3.8	4324	(0.15, 0.08)	434
B4	3.2	5.1/4.0	4.4/2.4	4.7/3.6	6152	(0.14, 0.14)	454

[a] Turn-on voltage at 1 cd m^{-2}. [b] η_C, η_P, and η_{ext} are the current, power, and external quantum efficiencies, respectively, inorder of maximum, and then values at 1000 cd m^{-2}. [c] The maximum luminance. [d] CIE is the Commission Internationale de L'Eclairage at 1000 cd m^{-2}. Device configurations: ITO/NPB (40 nm)/**Cz-TAn-DMAC** (20 nm)/TPBI (40 nm)/LiF (1 nm)/Al (device B1); ITO/NPB (40 nm)/**TPA-TAn-DMAC** (20 nm)/TPBI (40 nm)/LiF (1 nm)/Al (device B2); ITO/HATCN (10 nm)/NPB (40 nm)/TCTA (5 nm)/10 wt% **Cz-TAn-DMAC**: CBP (20 nm)/TPBI (40 nm)/LiF (1 nm)/Al (device B3); ITO/HATCN (10 nm)/NPB (40 nm)/TCTA (5 nm)/10 wt% **TPA-TAn-DMAC**: CBP (20 nm)/TPBI (40 nm)/LiF (1 nm)/Al (device B4).

space-limited-current (SCLC) method. Electron- and hole-only devices with configurations of ITO/NPB (10 nm)/**Cz-TAn-DMAC** or **TPA-TAn-DMAC** (80 nm)/NPB (10 nm)/Al and ITO/TPBI (10 nm)/**Cz-TAn-DMAC** or **TPA-TAn-DMAC** (80 nm)/TPBI (10 nm)/LiF (1 nm)/Al, respectively, are fabricated. Herein, thin layers of TPBI (electron mobility = 3.3 × 10^{-5} cm^2 V^{-1} s^{-1})[56] and NPB (hole mobility = 5.0 × 10^{-4} cm^2 V^{-1} s^{-1})[57] are used as buffer layers between the emitters and the electrodes. Considering the much thicker emitters layer (80 nm), the influence of thin buffer layers with higher carrier mobilities can be excluded during the calculation, and the mobility results primarily reflect the intrinsic properties of **Cz-TAn-DMAC** and **TPA-TAn-DMAC**.[58]

Fig. 4A shows the current density–voltage (J–V) characteristics of electron- and hole-only devices based on **Cz-TAn-DMAC** and **TPA-TAn-DMAC**. The J–V behaviors show ohmic characteristics. With increase in voltage, the current density grows into space-charge limited, which is quadratically dependent on the applied voltage. The SCLC characteristics can be dealt with by the reported ways.[25,29] Fig. 4B shows the field-dependent hole and electron mobilities.[25,29] Under an electric field of 5.5 × 10^5 V cm^{-1} the respective hole and electron mobilities are 6.6 × 10^{-6} and 2.4 × 10^{-5} cm^2 V^{-1} s^{-1} for the **Cz-TAn-DMAC**, and 2.0 × 10^{-4} and 8.2 × 10^{-5} cm^2 V^{-1} s^{-1} for the **TPA-TAn-DMAC**. Basically, the **Cz-TAn-DMAC** and **TPA-TAn-DMAC** show relatively balanced bipolar carrier transporting feature; however, the **TPA-TAn-DMAC** has faster electron and hole mobilities than the **Cz-TAn-DMAC**, which is beneficial to improve the EL performance.[59]

Hybrid WOLEDs

To obtain the full benefit of the excellent EL performance and bipolar carrier-transporting feature of **TPA-TAn-DMAC**, two-color hybrid WOLEDs comprising the doped film of orange phosphorescent Ir(tptpy)$_2$acac(iridium(III)bis(4-(4-*tert*-butylphenyl)thieno[3,2-*c*]pyridinato-N,C$^{2'}$)acetylacetonate) and neat film of the blue fluorescent **TPA-TAn-DMAC** are fabricated with a configuration of ITO/HATCN (5 nm)/NPB (40 nm)/TCTA (5 nm)/TCTA : Bepp$_2$: 3 wt% Ir(tptpy)$_2$acac(12 nm)/interlayer (3 nm)/**TPA-TAn-DMAC** (8 nm)/TPBI (40 nm)/LiF (1 nm)/Al. Moreover, the interlayer is composed of TCTA and Bepp$_2$ (bis[2-(2-hydroxyphenyl)-pyridine] beryllium) with different ratios. TCTA and Bepp$_2$ possess excellent hole- and electron-transporting abilities, respectively. The interlayer has the function of not only transporting carriers but also preventing harmful energy transfer from the phosphorescent layers to the fluorescent ones, due to the high triplet (T_1) energy levels of TCTA (2.82 eV)[60] and Bepp$_2$ (2.6 eV).[61] Furthermore, the high T_1 energy levels of TCTA and Bepp$_2$ make them possible co-host for the phosphors. Furthermore, the weight ratios of TCTA and Bepp$_2$ in both the interlayer and host can be adjusted, which plays a vital role in regulating the diffusions of carriers and excitons (Fig. 5). By changing these ratios, the distribution of exciton recombination areas in the blue and orange layers can be adjusted. Consequently, the color of WOLEDs can be tuned in a regular way.

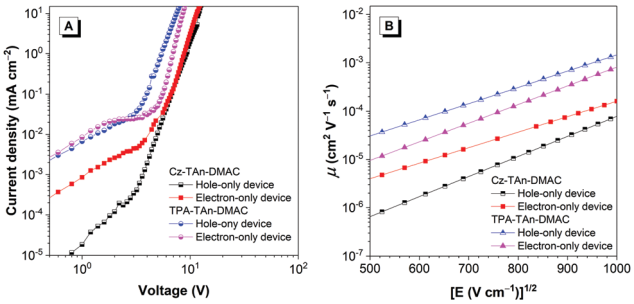

Fig. 4 (A) Plots of current density *versus* applied voltage of the devices, and (B) electric field-dependent hole and electron mobilities (μ) of both compounds.

When the weight ratio of the co-host of TCTA : Bepp$_2$ is maintained at 0.67 : 0.3, a series of WOLEDs (W1, W2, W3 and W4) are prepared by changing the component ratios of the interlayers. As shown in Table 3, the device W1 with an interlayer of sole TCTA radiates white light with color rendering index (CRI) of 53 at 5000 cd m^{-2} and displays maximum EL efficiencies of 22.9 cd A^{-1}, 15.1 lm W^{-1}, and 8.4%, which are maintained at close values of 22.5 cd A^{-1}, 12.6 lm W^{-1}, and 8.0% at 10 000 cd m^{-2}, indicating high stability of the device efficiencies. Nevertheless, the efficiencies of device W1 are not high enough, which is probably due to the fact that too many holes pass through the interlayer to the blue emission region and participate in the exciton recombination, while some of the electrons are blocked outside the orange emission layer by the interlayer. Hence, to improve the efficiencies, the electron

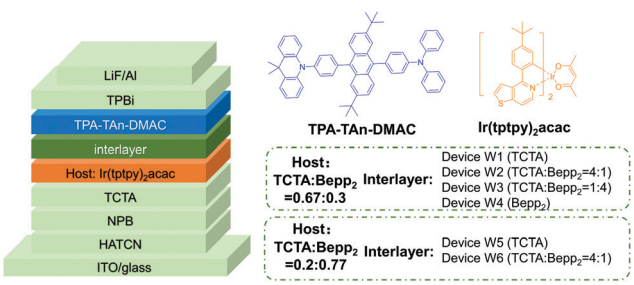

Fig. 5 Magnification configuration of two-color hybrid white OLEDs and the chemical structures of two emitters.

Table 3 EL performance of the WOLEDs based on **TPA-TAn-DMAC**

Device	V_{on}[a] (V)	L[b] (cd m^{-2})	η_C[c] (cd A^{-1})	η_{ext}[c] (%)	η_P[c] (lm W^{-1})	CRI[d]	CIE[d] (x, y)
W1	3.0	37 000	22.9/22.9/22.5	8.4/8.4/8.0	15.1/14.4/12.6	53	(0.37, 0.40)
W2	3.0	57 840	31.3/30.8/31.3	10.6/10.6/10.6	20.1/20.1/18.9	45	(0.41, 0.44)
W3	3.0	66 430	39.6/39.4/39.0	13.1/13.1/12.8	26.4/25.8/23.5	42	(0.42, 0.46)
W4	3.0	76 200	46.1/46.1/45.5	14.7/14.7/14.3	31.9/31.4/27.5	38	(0.44, 0.48)
W5	3.2	62 540	48.2/48.2/47.3	15.1/15.1/14.7	31.8/30.3/27.5	37	(0.44, 0.49)
W6	3.0	64 720	51.1/51.1/50.9	15.8/15.8/15.7	33.2/32.1/29.6	37	(0.44, 0.49)

[a] V_{on} is the turn-on voltage, which is measured at 1 cd m^{-2}. [b] L is the maximum luminance. [c] η_C, η_P, and η_{ext} are the current, power, and external quantum efficiencies, respectively, in order of maximum, then values at 5000, and 10 000 cd m^{-2}. [d] CRI and CIE is the color rendering index and the Commission Internationale de L'Eclairage, respectively, obtained at 5000 cd m^{-2}.

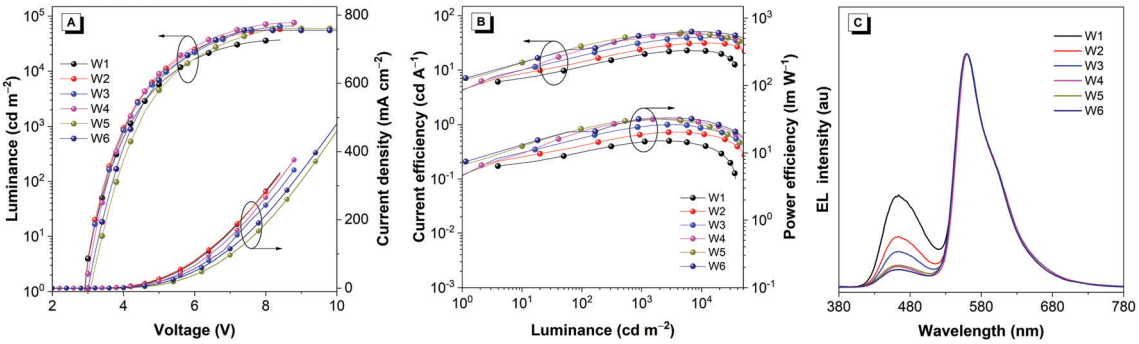

Fig. 6 (A) Luminance–voltage–current density curves, (B) current efficiency–luminance–power efficiency characteristic, and (C) EL spectra (measured at 6 V) of devices W1–W6.

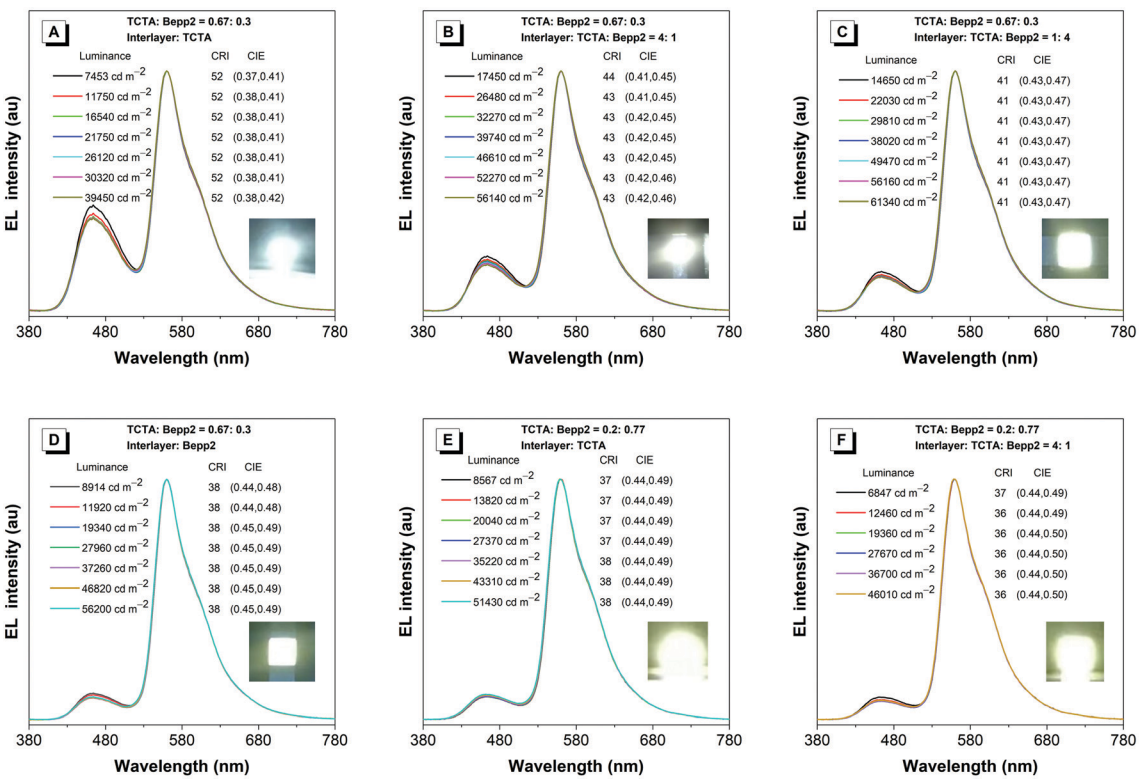

Fig. 7 ELspectra of the WOLEDs at varied luminance (A–F correspond to devices W1–W6).

transfer ability of the interlayer is gradually enhanced by increasing the ratio of $Bepp_2$ in the interlayer. By this way, more and more electrons pass through the interlayer to the region of phosphorescent orange emission layer and participate in the exciton recombination. Obviously, from W2 to W3 and W4, the weight percentages of $Bepp_2$ in the interlayer are increased from 20 wt% to 80 wt% and 100 wt%. In consequence, compared with W1, there are significant improvements in the EL efficiency, despite slight decrease in the CRI values. Notably, when the interlayer comprises $Bepp_2$ only, and the device W4 reaches the excellent maximum EL efficiencies of 46.1 cd A^{-1}, 31.4 lm W^{-1}, and 14.7% at 5000 cd m^{-2}, and maintains the high values of 45.5 cd A^{-1}, 27.5 lm W^{-1}, and 14.3% at 10 000 cd m^{-2}. Moreover, the maximum luminance of device W4 can exceed 70 000 cd m^{-2}. These results are in good agreement with our expectation.

To investigate the impact of the ratio of TCTA : $Bepp_2$ in the co-host on EL performance, devices W5 and W6 with the co-host of TCTA : $Bepp_2$ (0.2 : 0.77) and interlayer of TCTA and TCTA : Bepp2 (4 : 1), respectively, are fabricated. Significantly, for device W1 and W5, although they have the same composition of interlayer, the EL colors and efficiencies are quite different, which reveals that besides the interlayer, the ratio of co-host can work on regulation of the exciton recombination region. Device W6 achieves the best EL performance of 51.1 cd A^{-1}, 32.1 lm W^{-1}, 15.8% at about 5000 cd m^{-2}, and realizes the emission of low-blue and eye-caring white light. Note that when the luminance increases from 5000 to 10 000 cd m^{-2}, there is virtually no efficiency loss (Fig. 6). Even at a much higher luminance of 30 000 cd m^{-2}, η_{ext} still remains at 14.3%, indicative of a very promising prospect of practical application. More importantly, for the hybrid WOLEDs, apart from the permanence of efficiency, the stability of emission spectra is very essential. As shown in Fig. 7, for devices W1–W6, they all possess very stable spectra, and the (x, y) of CIE coordinates vary less than (0.01, 0.01) from 5000 to 30 000 cd m^{-2} or higher, which is attributed to the relatively balanced carrier transport and stable recombination region of the excitons.

Conclusions

In summary, two new luminescent compounds, **Cz-TAn-DMAC** and **TPA-TAn-DMAC**, comprising an anthracene core with branched *tert*-butyl groups and functional electron-donating groups are synthesized and fully characterized. They possess high thermal stability and bipolar charge transport ability and exhibit strong deep-blue emissions at 449 and 459 nm with good Φ_F values of 41.7% and 53.7% in neat films. The non-doped device based on **TPA-TAn-DMAC** radiates bright deep-blue light ($CIE_{x,y}$ = 0.14, 0.18) with a high $\eta_{ext,max}$ of 4.9%, and the doped OLED based on **Cz-TAn-DMAC** displays stable bluer emission ($CIE_{x,y}$ = 0.15, 0.08) with a $\eta_{ext,max}$ of 4.8%. The TTF process is accountable for the high $\eta_{exciton}$ values over 25% and thus $\eta_{ext,max}$ values. Moreover, by controlling the compositions of the co-host and interlayer, high-performance two-color hybrid WOLEDs are achieved based on **TPA-TAn-DMAC** and an orange phosphorescent emitter, thus affording ultra-high spectral stability and efficiency stability. The excellent EL performances of these compounds in deep-blue OLEDs and WOLEDs clearly manifest their high potentials in display and lighting devices.

Conflicts of interest

There is no conflict to declare.

Acknowledgements

This work was financially supported by the National Natural Science Foundation of China (21788102), the Natural Science Foundation of Guangdong Province (2019B030301003), the Research Grants Council of Hong Kong (16305518) and the Fundamental Research Funds for the Central Universities.

Notes and references

1 H. Wu, J. Zeng, Z. Xu, B. Zhang, H. Zhang, Y. Pan, Z. Wang, D. Ma, A. Qin and B. Z. Tang, *J. Mater. Chem. C*, 2019, **7**, 13047–13051.
2 Z. Xu, Y. Gong, Y. Dai, Q. Sun, X. Qiao, D. Yang, X. Zhan, Z. Li, B. Z. Tang and D. Ma, *Adv. Opt. Mater.*, 2019, **7**, 1801539.
3 Z. Xu, J. Gu, X. Qiao, A. Qin, B. Z. Tang and D. Ma, *ACS Photonics*, 2019, **6**, 767.
4 H. Zhang, J. Zeng, W. Luo, H. Wu, C. Zeng, K. Zhang, W. Feng, Z. Wang, Z. Zhao and B. Z. Tang, *J. Mater. Chem. C*, 2019, **7**, 6359–6368.
5 J. Zhao, Z. Yang, X. Chen, Z. Xie, T. Liu, Z. Chi, Z. Yang, Y. Zhang, M. P. Aldred and Z. Chi, *J. Mater. Chem. C*, 2018, **6**, 4257–4264.
6 Z. Xu, J. Gu, J. Huang, C. Lin, Y. Li, D. Yang, X. Qiao, A. Qin, Z. Zhao, B. Z. Tang and D. Ma, *Mater. Chem. Front.*, 2019, **3**, 2652–2658.
7 P. Han, Z. Xu, C. Lin, D. Ma, A. Qin and B. Z. Tang, *J. Mater. Chem. C*, 2020, **8**, 7012–7018.
8 P. Therdkatanyuphong, C. Kaiyasuan, P. Chasing, T. Kaewpuang, T. Chawanpunyawat, T. Sudyoadsuk and V. Promarak, *ACS Appl. Electron. Mater.*, 2021, **3**, 1311–1322.
9 X. Lv, L. Xu, W. Cui, Y. Yu, H. Zhou, M. Cang, Q. Sun, Y. Pan, Y. Xu and D. Hu, *ACS Appl. Mater. Interfaces*, 2020, **13**, 970–980.
10 X. Liu, W. Liu, D. Wu, X. Wei, L. Wang, H. Wang, Y. Miao, H. Xu, J. Yu and B. Xu, *J. Mater. Chem. C*, 2020, **8**, 14117–14124.
11 M. Zhang, K. Wang, C. Zheng, W. Liu, H. Lin, S. Tao and X. Zhang, *Org. Electron.*, 2017, **50**, 466–472.
12 J. Zhao, S. Yuan, X. Du, W. Li, C. Zheng, S. Tao and X. Zhang, *Adv. Opt. Mater.*, 2018, **6**, 1800825.

13 C. Xue, H. Lin, G. Zhang, Y. Hu, W. Jiang, J. Lang, D. Wang and G. Xing, *J. Mater. Sci.: Mater. Electron.*, 2020, **31**, 4444–4462.
14 J. Zeng, J. Guo, H. Liu, Z. Zhao and B. Z. Tang, *Adv. Funct. Mater.*, 2020, **30**, 2000019.
15 X. Cai and S. Su, *Adv. Funct. Mater.*, 2018, **28**, 1802558.
16 X. Du, J. Zhao, S. Yuan, C. Zheng, H. Lin, S. Tao and C. Lee, *J. Mater. Chem. C*, 2016, **4**, 5907–5913.
17 K. Lee and J. Lee, *Adv. Opt. Mater.*, 2020, **8**, 2000328.
18 C. Zheng, J. Wang, J. Ye, M. Lo, X. Liu, M. Fung, X. Zhang and C. Lee, *Adv. Mater.*, 2013, **25**, 2205–2211.
19 C. Cao, W. Chen, J. Chen, L. Yang, X. Wang, H. Yang, B. Huang, Z. Zhu, Q. Tong and C. Lee, *ACS Appl. Mater. Interfaces*, 2019, **11**, 11691–11698.
20 H. J. Jang, J. Y. Lee, J. Kwak, D. Lee, J. Park, B. Lee and Y. Y. Noh, *J. Inf. Disp.*, 2020, **20**, 1–8.
21 Q. Zhang, J. Li, K. Shizu, S. Huang, S. Hirata, H. Miyazaki and C. Adachi, *J. Am. Chem. Soc.*, 2012, **134**, 14706–14709.
22 X. Cai, B. Gao, X. Li, Y. Cao and S. Su, *Adv. Funct. Mater.*, 2016, **26**, 8042–8052.
23 X. Cao, D. Zhang, S. Zhang, Y. Tao and W. Huang, *J. Mater. Chem. C*, 2017, **5**, 7699–7714.
24 Y. Chen, Q. Sun, Y. Dai, D. Yang, X. Qiao and D. Ma, *J. Mater. Chem. C*, 2020, **8**, 13777–13785.
25 Y. Li, Z. Xu, X. Zhu, B. Chen, Z. Wang, B. Xiao, J. W. Y. Lam, Z. Zhao, D. Ma and B. Z. Tang, *ACS Appl. Mater. Interfaces*, 2019, **11**, 17592–17601.
26 K. Matsuo and T. Yasuda, *Chem. Sci.*, 2019, **10**, 10687–10697.
27 X. Ning, C. Zhao, B. Jiang, S. Gong, D. Ma and C. Yang, *Dyes Pigm.*, 2019, **164**, 206–212.
28 J. L. Segura, *Acta Polym.*, 1998, **49**, 319–344.
29 B. Chen, B. Liu, J. Zeng, H. Nie, Y. Xiong, J. Zou, H. Ning, Z. Wang, Z. Zhao and B. Z. Tang, *Adv. Funct. Mater.*, 2018, **28**, 1870288.
30 M. Aydemir, G. Haykir, A. Battal, V. Jankus, S. K. Sugunan, F. B. Dias, H. Al-Attar, F. Turksoy, M. Tavasli and A. P. Monkman, *Org. Electron.*, 2016, **30**, 149–157.
31 I. Cho, S. H. Kim, J. H. Kim, S. Park and S. Y. Park, *J. Mater. Chem.*, 2012, **22**, 123–129.
32 J. Huang, J. Su and H. Tian, *J. Mater. Chem.*, 2012, **22**, 10977–10989.
33 H. Park, J. Lee, I. Kang, H. Y. Chu, J. I. Lee, S. K. Kwon and Y. H. Kim, *J. Mater. Chem.*, 2012, **22**, 2695–2700.
34 P. Han, C. Lin, D. Ma, A. Qin and B. Z. Tang, *ACS Appl. Mater. Interfaces*, 2020, **12**, 46366–46372.
35 Y. Zheng, Z. Wang, X. Wang, J. Li, X. Feng, G. He, Z. Zhao and H. Lu, *ACS Appl. Electron. Mater.*, 2021, **3**, 422–429.
36 J. Shi and C. W. Tang, *Appl. Phys. Lett.*, 2002, **80**, 3201–3203.
37 A. Slodek, M. Filapek, E. Schab-Balcerzak, M. Grucela, S. Kotowicz, H. Janeczek, K. Smolarek, S. Mackowski, J. G. Malecki, A. Jedrzejowska, G. Szafraniec-Gorol, A. Chrobok, B. Marcol, S. Krompiec and M. Matussek, *Eur. J. Org. Chem.*, 2016, 4020–4031.
38 B. Yang, S. Kim, H. Xu, Y. Park, H. Zhang, C. Gu, F. Shen, C. Wang, D. Liu and X. Liu, *ChemPhysChem*, 2008, **9**, 2601–2609.
39 A. Chaskar, H. Chen and K. T. Wong, *Adv. Mater.*, 2011, **23**, 3876–3895.
40 H. Liu, L. Kang, J. Li, F. Liu, X. He, S. Ren, X. Tang, C. Lv and P. Lu, *J. Mater. Chem. C*, 2019, **7**, 10273–10280.
41 Y. Shen, H. Liu, S. Zhang, Y. Gao, B. Li, Y. Yan, Y. Hu, L. Zhao and B. Yang, *J. Mater. Chem. C*, 2017, **5**, 10061–10067.
42 L. Wang, G. Lei and Y. Qiu, *J. Appl. Phys.*, 2005, **97**, 114503.
43 V. V. Patil, K. H. Lee and J. Y. Lee, *Dyes Pigm.*, 2020, **174**, 108070.
44 G. Chen, W. Li, T. Zhou, Q. Peng, D. Zhai, H. Li, W. Yuan, Y. Zhang and B. Z. Tang, *Adv. Mater.*, 2015, **27**, 4496–4501.
45 C. Wang and Z. Li, *Mater. Chem. Front.*, 2017, **1**, 2174–2194.
46 X. Shen, Y. Wang, E. Zhao, W. Yuan, Y. Liu, P. Lu, A. Qin, Y. Ma, J. Sun and B. Z. Tang, *J. Phys. Chem. C*, 2013, **117**, 7334–7347.
47 Z. Li, T. Ye, S. Tang, C. Wang, D. Ma and Z. Li, *J. Mater. Chem. C*, 2015, **3**, 2016–2023.
48 M. Bian, Z. Zhao, Y. Li, Q. Li, Z. Chen, D. Zhang, S. Wang, Z. Bian, Z. Liu and L. Duan, *J. Mater. Chem. C*, 2018, **6**, 745–753.
49 V. V. Patil, K. H. Lee and J. Y. Lee, *Adv. Opt. Mater.*, 2020, **8**, 2000480.
50 D. Y. Kondakov, T. D. Pawlik, T. K. Hatwar and J. P. Spindler, *J. Appl. Phys.*, 2009, **106**, 124510.
51 R. Liu, Y. Zhang, Y. L. Lei, P. Chen and Z. H. Xiong, *J. Appl. Phys.*, 2009, **105**, 093719.
52 X. Guo, P. Yuan, J. Fan, X. Qiao, D. Yang, Y. Dai, Q. Sun, A. Qin, B. Z. Tang and D. Ma, *Adv. Mater.*, 2021, **33**, 2006953.
53 X. Guo, P. Yuan, X. Qiao, D. Yang, Y. Dai, Q. Sun, A. Qin, B. Z. Tang and D. Ma, *Adv. Funct. Mater.*, 2020, **30**, 1908704.
54 T. C. Tsai, W. Y. Hung, L. C. Chi, K. T. Wong, C. C. Hsieh and P. T. Chou, *Org. Electron.*, 2009, **10**, 158–162.
55 J. Seo, S. Jeon and J. Lee, *Org. Electron.*, 2016, **34**, 33–37.
56 W. X. Shi, N. Liu, Y. M. Zhou and X. A. Cao, *IEEE Trans. Electron Devices*, 2019, **66**, 1057–1062.
57 Q. Du, W. Wang, S. Li, D. Zhang, W. Li and W. Zheng, *Opt. Commun.*, 2016, **366**, 253–259.
58 Z. Li, Z. Cheng, J. Lin, N. Xie, C. Li, G. Yang and Y. Wang, *J. Mater. Chem. C*, 2019, **7**, 13486–13492.
59 S. Hu, J. Zeng, X. Zhu, J. Guo, S. Chen, Z. Zhao and B. Z. Tang, *ACS Appl. Mater. Interfaces*, 2019, **11**, 27134–27144.
60 Y. S. Tsai, L. A. Hong, F. S. Juang, C. Y. Cheng and D. G. Wang, *J. Nanosci. Nanotechnol.*, 2016, **16**, 11750–11756.
61 J. Chen, F. Zhao and D. Ma, *Mater. Today*, 2014, **17**, 175–183.